Impact of intermittent gravity wave activity on the middle atmospheric circulation during boreal winter

Samtleben N. and Jacobi Ch.

Institute for Meteorology, Universität Leipzig, Stephanstraße 3, 04103 Leipzig, Germany
Email: Nadja.Samtleben@uni-leipzig.de

Summary: Simulations of the circulation in the middle atmosphere during northern winter performed with a nonlinear, mechanistic, global circulation model show that the upper mesospheric jet is greatly overestimated and also the position with respect to latitude and height does not correspond to observations. Apart from that also the winter wind reversal in the mesopause region, evoked by breaking gravity waves (GWs), is located too low around 80 km, but is observed to be usually around 100 km. These discrepancies are planned to be eliminated by modifying the distribution of GW amplitudes driving the GW parameterization. This distribution is currently based on potential GW energy data derived from GPS radio occultation measurements and has to be replaced by a distribution based on momentum flux estimates applying midfrequency approximation. The results show a weaker mesospheric jet more realistically tilted towards lower latitudes with height. Also the meridional circulation extending from the summer to the winter pole decelerates and less GWs are propagating into the mesosphere. By additionally varying the GW amplitudes in magnitude and time, the wind reversal is shifted upwards and the mesospheric jet is slowed down.

Zusammenfassung: Simulationen der Zirkulation der mittleren Atmosphäre während des nordhemisphärischen Winters unter Verwendung eines nicht-linearen mechanistischen globalen Zirkulationsmodells ergaben beim Vergleich mit Messungen, dass der simulierte, mesosphärische Jet stark überschätzt wird und dessen Position von den Beobachtungen abweicht. Die in der Mesopausenregion einsetzende Windumkehr, hervorgerufen durch brechende Schwerewellen, befindet sich in etwa 80 km anstatt in 100 km. Diese Diskrepanzen sollen eliminiert werden. Hierfür wird die Verteilung der Schwerewellenamplituden, die die Schwerewellenparametrisierung innerhalb des Modells antreibt, am oberen Rand der Troposphäre modifiziert. Diese basiert derzeit auf global beobachteten, zonal gemittelten Daten der potentiellen Energie von Schwerewellen abgeleitet aus GPS Radiookkultationsmessungen und soll durch eine auf Impulsflüssen basierende Verteilung ersetzt werden. Das Modellexperiment zeigt, dass der mesosphärische Jet mit der Höhe in Richtung niedriger Breiten geneigt ist und abgebremst wird. Zudem schwächt die Meridionalzirkulation vom Sommer- zum Winterpol leicht ab und weniger Schwerewellen dringen bis in die Mesosphäre vor. Zusätzlich wird durch zeitliche und unterschiedlich starke Variation der Schwerewellenamplitude die Windumkehr verlagert und der mesosphärische Jet abgebremst.

1. Introduction

The dynamics in the middle atmosphere are mainly dominated by the stratospheric and mesospheric jet and also by the impact of atmospheric waves with different spatial and temporal scales. The most important characteristic of atmospheric waves is their ability to transport and deposit energy and momentum from their origin. In particular gravity waves (GWs) distribute energy and momentum throughout the whole atmosphere thereby maintaining the circulation and the thermal structure of the upper atmosphere. They also contribute to turbulence and mixing between all vertical layers. GWs mainly develop in the troposphere [Fritts and Alexander, 2003]. Strongly depending on the phase speed c and the background wind u, GWs are able to propagate into the middle atmosphere. Their amplitude is exponentially increasing with height due to the exponentially decreasing density of the atmosphere. Usually, the GW spectrum is already saturated in the stratosphere which means that GW amplitudes cannot grow anymore and, according to the linear theory, partly break. This effect is the stronger the closer their phase speed c is to the background wind u. If $c=u$, the GW encounters its critical line and cannot propagate anymore. Thus, mainly GWs propagating into the opposite direction than the background wind are frequently observed in the middle atmosphere. Also GWs being faster than the background wind are able to propagate but they are filtered out by the strong mesospheric jet at the latest. For this reason the wind reverses in the mesosphere due to GW breaking, while in the opposite direction to u traveling GWs depositing their momentum [Lindzen, 1981; Holton, 1982].

Due to the huge amount of different trigger mechanisms GWs have a large spatial and temporal variability. They are not distributed homogenously and exhibit a large intermittency which is closely linked to the synoptic conditions, the source of the GWs and the propagation conditions. To capture the irregular global distribution of GWs the momentum flux (MF) is estimated by using satellite data [Ern et al., 2004; Preusse et al., 2006; Fröhlich et al., 2007; Schmidt et al., 2016] as well as the potential energy (E_{pot}), a proxy for GW activity. The potential energy can be derived from GPS radio occultation (RO) density [e.g. Šácha et al., 2015, 2016] or temperature [Ratnam et al., 2004a, b; Schmidt et al., 2016] measurements that are based on radio links between a low-earth orbiting satellite and a GPS satellite. To study specific characteristics like the phase speed, the wavelength, the wavenumber or the temporal development of the GW activity with a certain precision other measurements like lidar [Baumgarten et al., 2015; Witschas et al., 2017], radar [Gavrilov and Fukao, 1999; Oleynikov et al., 2005] or balloon measurements [Hertzog et al., 2012; Plougonven et al., 2012] are performed.

Based on this gained knowledge it is still complicated and extremely computer-time consuming to resolve GWs in global circulation models (GCMs). GWs have horizontal wavelengths of tens to hundreds of kilometers so that most of the GWs are subgrid scale due to the coarse resolution of GCMs. For this reason GWs are mostly parameterized by integrating a GW distribution in the lower part of the atmosphere either based on GW source parameterizations, or on specific functions or observed GW fields [Šácha et al., 2016; Lilienthal et al., 2017], especially from satellite data.

In this paper, we modify the prescribed GW field based on E_{pot} data from GPS RO density measurements [Šácha et al., 2015] by another one based on MF estimates that

have been derived from these E_{pot} field applying midfrequency approximation [Ern et al., 2004]. Also the distribution of small and large GW amplitudes and their temporal sequence are adapted. The aim is to create a more realistic model climatology of the middle atmosphere.

2. MUAM - Model description

MUAM [Pogoreltsev et al., 2007; Jacobi et al., 2015] is a non-linear mechanistic 3D grid point model which is an updated version of the global circulation model COMMA-LIM [Fröhlich et al., 2003a, b; Jacobi et al., 2006]. The model has a horizontal resolution of 5° in latitude and 5.625° in longitude. It has 56 vertical levels up to a logarithmic pressure height of about 160 km with a vertical resolution of 2.842 km and a scale height of H = 7 km. At 1000 hPa, the lower boundary of the model, stationary waves of zonal wavenumbers 1 to 3 are forced, which are extracted from 2000-2010 ERA Interim temperature and geopotential reanalysis data. Up to 30 km the zonal mean model temperature is nudged to zonal mean ERA Interim temperatures to correct the climatology of the troposphere, which is otherwise not included in the model. The model solves the primitive equations in flux form [Jakobs et al., 1986]. It includes parameterizations of solar radiation [Strobel, 1986], infrared cooling [Fomichev, 1998], and GWs. The latter are parameterized with an updated linear scheme [Lindzen, 1981; Jakobs et al., 1986] with multiple breaking levels [Fröhlich et al., 2003a, b; Jacobi et al., 2006]. Once a GW becomes unstable, the amplitude saturates and stops increasing exponentially with height. The MF is simultaneously reduced and the zonal mean flow is accelerated. The GW can have multiple saturation levels until the GW reaches a critical line and the MF becomes equal to zero. GW amplitudes are initialized at an altitude of 10 km as zonal mean with a global average of 1 cms^{-1} for the vertical velocity perturbation. In the standard configuration this value is weighted by a prescribed global GW amplitude distribution based on E_{pot} data obtained from GPS radio occultation measurements [Lilienthal et al., 2017]. At each grid point 48 waves are induced propagating in eight different directions with six different phase speeds.

Fig. 1 shows the zonal (a) and meridional wind (b), the temperature (c), zonal GW flux (d) and acceleration due to breaking GWs (e) in January as a latitude-height plot. The meridional circulation has a maximum of 4 ms^{-1} at about 80 km. This circulation leads to a warming/cooling of the winter/summer mesosphere (Fig. 1c) due to descending/ascending air. The northern hemisphere (NH) mesopause temperature is much higher than on the southern hemisphere (SH). The winter stratosphere is dominated by the polar vortex during polar night. The temperature becomes smaller than 210 K. In the summer stratosphere the temperature increases with height due to absorption of solar radiation by ozone and reaches a maximum of more than 270 K near the stratopause. As a result of the development of the stratospheric low pressure system above the pole on the NH and the increasing pressure and temperature towards lower latitudes, a west wind establishes with a maximum of about 50 ms^{-1} (Fig. 1(a)). Compared to reference climatologies like CIRA-86 [Fleming et al., 1988] or URAP [Swinbank and Ortland, 2003] (see Fig. 7 below) the jet is overestimated by more than 10 ms^{-1}. The mesospheric jet in climatologies is additionally tilted towards lower latitudes with

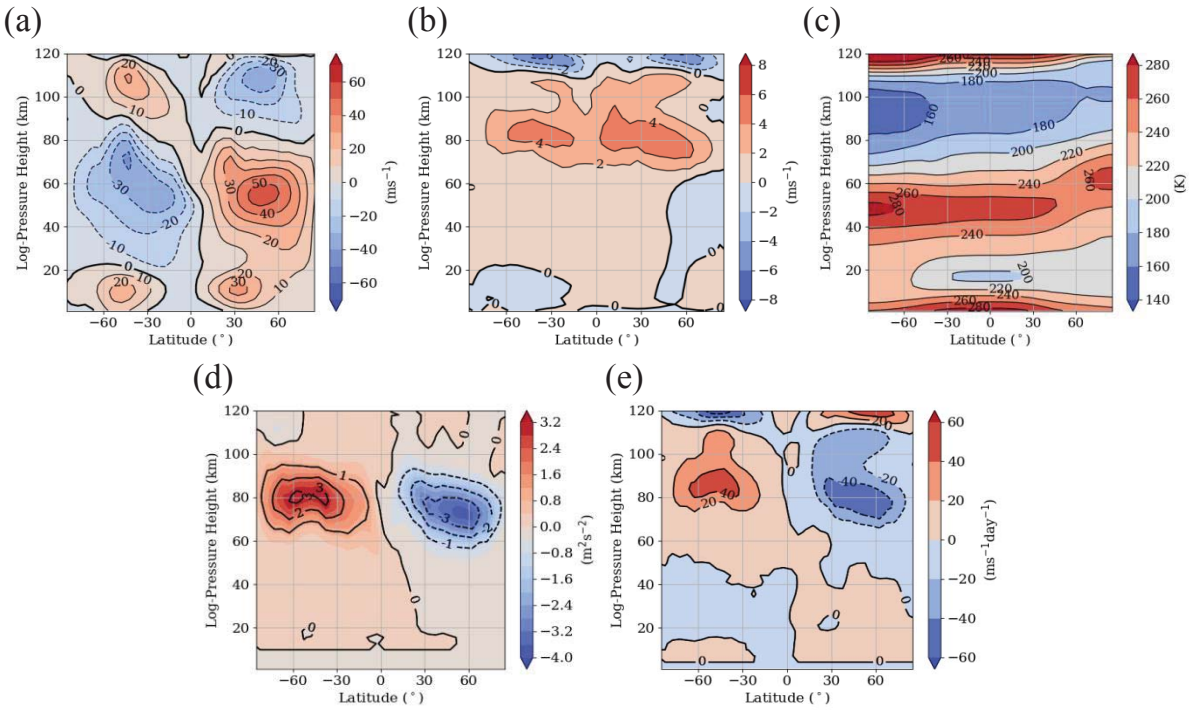

Figure 1: January zonal and monthly mean of the (a) zonal wind [ms^{-1}], (b) meridional wind [ms^{-1}], (c) temperature [K], (d) GW fluxes [m^{2}s^{-2}]and (e) acceleration through breaking GWs [ms^{-1}day^{-1}]. GW parameterization is based on E_{pot} data (standard configuration).

increasing altitude but this cannot be observed in the MUAM standard configuration results. The wind reversal above 80 km is due to breaking GWs. GW fluxes and acceleration due to breaking GWs are shown in Figs. 1(d) and (e).

3. Initialisation of gravity waves in the upper troposphere in MUAM

3.1. Different distributions of gravity wave amplitudes as zonal mean

Instead of using the GW distribution based on the observed E_{pot} data we calculated the MF distribution by applying midfrequency approximation according to Ern et al. [2004]. Therefore, the horizontal momentum flux F_h can be assigned to E_{pot} multiplied with the ratio of the horizontal and vertical wavenumbers k and m [Ern et al., 2004]:

$$F_h = \frac{1}{2}\rho\frac{k}{m}\left(\frac{g}{N}\right)^2\left(\frac{\hat{T}}{T}\right)^2 \qquad \left| \quad E_{pot} = \frac{g^2\hat{T}^2}{2N^2T^2} \right. \tag{1}$$

$$F_h = \rho\frac{k}{m}E_{pot} \tag{2}$$

Here, g is the acceleration due to gravity, N is the buoyancy frequency, ϱ is the density, T is the background temperature and $\hat{T}$ is the deviation of the temperature T. To eliminate the term with the horizontal and vertical wavenumber we are using the dispersion relation valid in the midfrequency approximation (Eq. 3). Following Preusse et al. [2006] we set the ratio of the intrinsic frequency $\hat{\omega}$ and the Coriolis parameter f equal to 3. Thus, we can replace the intrinsic frequency $\hat{\omega}$ by $3f$:

$$\hat{\omega}^2 = \frac{N^2 k^2}{m^2} \quad \left| \quad \frac{\hat{\omega}}{f} = 3 \longleftrightarrow \hat{\omega}^2 = 9 f^2 \right. \tag{3}$$

and obtain a relation of the ratio of the vertical and horizontal wavenumber *m* and *k* to the ratio of *f* and *N*:

$$9 f^2 = \frac{N^2 k^2}{m^2} \longleftrightarrow \frac{k}{m} = \frac{3 f}{N} \tag{4}$$

Combining Eqs. (2) and (4) provides the vertical MF by applying midfrequency approximation:

$$F_h = 3\rho \frac{f}{N} E_{pot} \tag{5}$$

Figure 2 shows the latitudinal distribution of initial vertical wind amplitudes based on E_{pot} (dotted line) and MF (solid line) data with a global mean of 1 cms^{-1}. The standard configuration by using E_{pot} provides higher values in the equatorial region due to convectively generated GWs, which, however, carry low MF and are therefore absent in the new configuration. The maxima in the midlatitudes represent the orographically induced GWs. These amplitudes are larger in the winter hemisphere than in the summer hemisphere. Using MF, the GW amplitudes are a bit larger, which is due to the normalization to the same global average of 1 cms^{-1} in the absence of an equatorial maximum due to $f \to 0$ there.

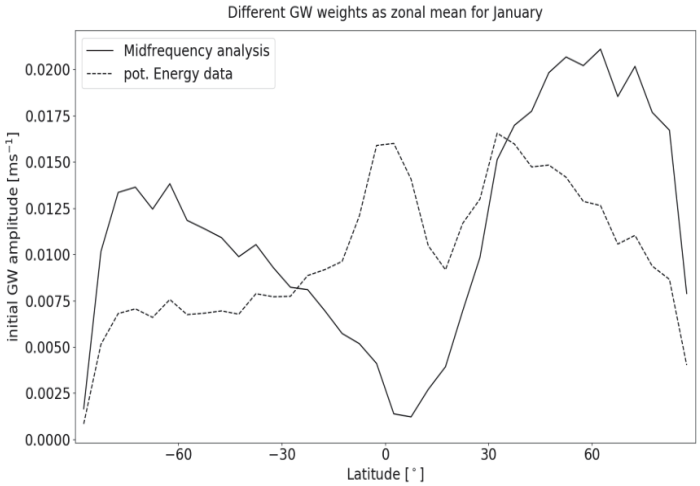

Figure 2: GW vertical wind amplitudes for the simulation based on the GPS RO E_{pot} (dotted line) and MF (solid line) data for January conditions.

3.2. Intermittent gravity wave activity

Hertzog et al. [2012] having performed in situ balloon measurements in the stratosphere for several months and found that the GW MF is unevenly distributed. They observed many GWs with small and only a few ones with large MFs. In the MUAM

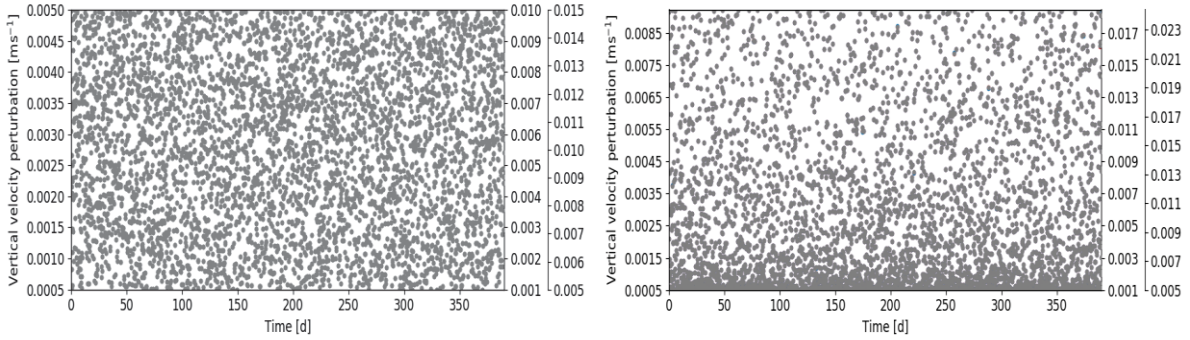

Figure 3: Linear (left) and x³ (right) distribution of the random numbers representing the variation of the vertical velocity perturbation with mean values of 1 cms^{-1}, 0.5 cms^{-1} and 0.275 cms^{-1}.

standard configuration, there is no temporal variation of the GWs excited in the troposphere. To create a more realistic distribution of the MF, based on the results of Hertzog et al. [2012] the GW amplitudes have been multiplied with randomly generated numbers in order to represent their temporal variability. These random numbers are shown in Fig. 3 for a whole simulation. They are distributed either linearly (left) or polynomially (order 3) (right) with mean values of 1 cms^{-1}, 0.55 cms^{-1} and 0.275 cms^{-1}, respectively representing larger or smaller mean amplitudes. The amplitudes for each mean value are based on the same set of random numbers, so that the chronology of large and small amplitudes is the same for each model experiment. For comparison experiments were also performed with the mean value kept constant. The aim is to slow down the mesospheric jet by GWs with larger amplitudes breaking at lower altitudes and to displace the wind reversal upwards by GWs with smaller amplitudes breaking at higher altitudes. Tab. 1 gives an overview of all simulations. The respective short name indicates which GW amplitude distribution was used (EP-potential energy and MF-momentum flux), which vertical velocity perturbation distribution was chosen (C-constant, L-linear and P-polynomial) and the respective minima, maxima and mean values.

Name	Distribution	Minimum (cms^{-1})	Maximum (cms^{-1})	Mean (cms^{-1})
EP-L-C	EP	1	1	1
MF-L-C	MF	1	1	1
MF-M-C	MF	0.55	0.55	0.55
MF-S-C	MF	0.275	0.275	0.275
MF-L-L	MF	0.5	1.5	1
MF-M-L	MF	0.1	1	0.55
MF-S-L	MF	0.05	0.5	0.275
MF-L-P	MF	0.5	2.4	1
MF-M-P	MF	0.1	1.8	0.55
MF-S-P	MF	0.05	0.9	0.275

Table 1: Overview of the model experiments based on E_{pot} data (EP) and on MF calculations (MF) for large (L), medium(M) or small (S) amplitudes and a constant (C), linear (L) and 3rd order polynomial (P) distribution.

4. Results of the simulations with modified gravity wave initialisation

4.1. Potential energy vs. momentum flux based GW distribution

In the first column of Fig. 4 the zonal (Ia) and meridional wind (Ib), the temperature (Ic), the GW flux (Id) and acceleration of the zonal wind due to breaking GWs (Ie) are presented for the MF-L-C1. By comparing Fig. 4(Ia) with Fig. 1(a) it can be seen that the zonal wind has changed. On the SH the mesospheric jet is slightly weaker. This is because GW amplitudes based on the MF distribution are larger on the SH. Thus, more large GWs are generated, which are not able to propagate into the upper mesosphere and thus, break in the stratosphere where they decelerate the mesospheric jet. Due to the small GW amplitudes in the equatorial region (Fig. 2) the wind reversal is lifted from 60 km to 80 km because small GWs are breaking in higher altitudes. As a result the SH mesospheric jet is somewhat shifted towards the NH, which is consistent with observations (see Fig. 7). Also the NH mesospheric jet with 50 ms^{-1} in maximum has changed significantly regarding shape and position. The whole west wind regime is tilted towards lower latitudes with increasing altitude. This also corresponds to observations (Fig. 7 below). However, the strength of the mesospheric jet did not decrease and the wind reversal in the mesosphere dropped from 80 km to 70 km at 50° N as result of the greater inclination of the west wind regime. There are no substantial changes of the meridional wind, except for the equatorial region, where the meridional wind increased above 80 km. The temperature distribution did not change significantly, too. The GW parameters are in good agreement with the zonal wind changes. Due to the displacement of the zero wind line in the equatorial region towards the NH more eastward directed GWs (positive GW flux - Fig. 4(Id)) can propagate and locally maintain the modified zonal wind conditions. The same effect can be observed on the NH. The area of the strongest westward directed GW flux is also tilted towards lower latitudes with increasing height and also preserves the tilt of the zonal wind. The incline can be observed as well in the acceleration through breaking GWs (Fig. 4(Ie)). The strength of the westward directed GW flux and of the acceleration due to GWs on the NH did not change which would be necessary to adjust the strength of the mesospheric jet.

4.2. Modification of the height of the wind reversal and the strength of the stratospheric jet

Figs. 4-6 show the results of the model experiments based on variable vertical velocity perturbations with different mean values and temporal distributions.
Fig. 4 presents the same parameters like in Fig. 1 for the simulations with large amplitudes MF-L-C (column I), MF-L-L (column II) and MF-L-P (column III). By comparing the five parameters of each approach in Fig. 4 no significant changes can be observed. On the NH the mesospheric jet is slightly decreasing with increasing maximum values of the vertical velocity perturbation distribution (from left I(a) to right III(a)). The maximum value of 2.4 cms^{-1} in the MF-L-P simulation generates large GWs breaking early but due to the polynomial distribution they do not occur frequently. Thus, the forcing of large GWs is too weak to significantly decrease the mesospheric jet. Due to the huge amount of small GWs, propagating to higher altitudes, the GW flux is enhanced on the NH. But still these kind of scaling factors are

too small to reduce the intensity of the mesospheric jet and too large to elevate the wind reversal in the mesosphere. Fig. 5 shows the results of the MF-M-C (I), MF-M-L (II) and MF-M-P (III) simulations. In general, the values of the vertical velocity perturbation are smaller than those of the approach in Fig. 4. So, it can be expected that the zonal wind is stronger and the wind reversal even higher. The MF-L-C run

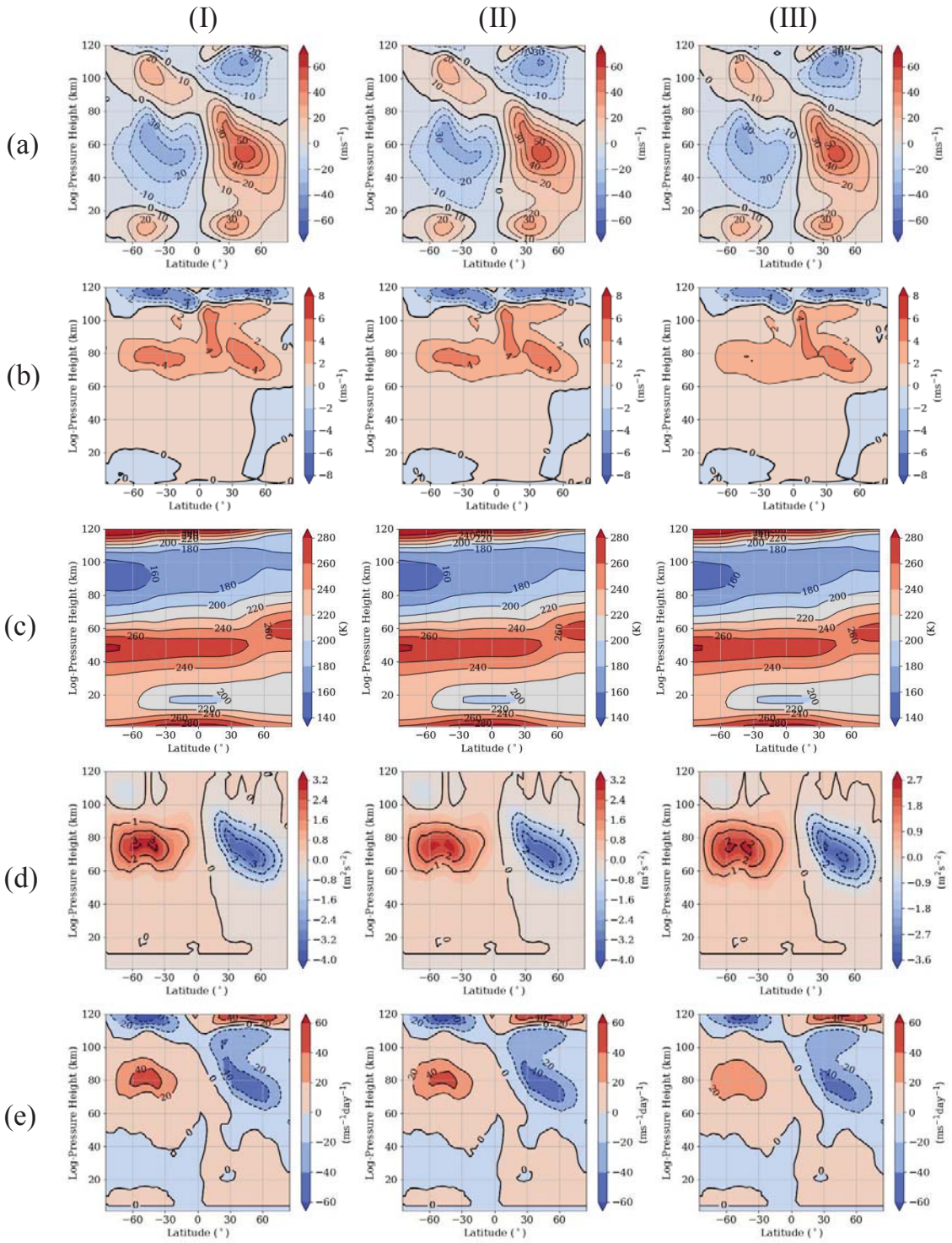

Figure 4: Zonal mean (a) zonal wind, (b) meridional wind, (c) temperature, (d) GW fluxes and (e) acceleration through GWs in the middle atmosphere for the MF-L-C (I) MF-L-L (II) and MF-L-P (III) simulations.

shows a mesospheric jet with 60 ms^{-1} in maximum and a wind reversal shifted by 10 km. The small GWs are able to propagate to higher altitudes where they break and relocate the wind reversal. This can be seen as well in the GW acceleration (Fig. 5 I(e)-III(e)) maximizing in the thermosphere. In this region also the meridional circulation (Fig. 5 I(b)-III(b)) is enhanced. The stratosphere is not affected by these GWs anymore. These effects can be reduced by the larger scaling factors in the polynomial and linear distribution.

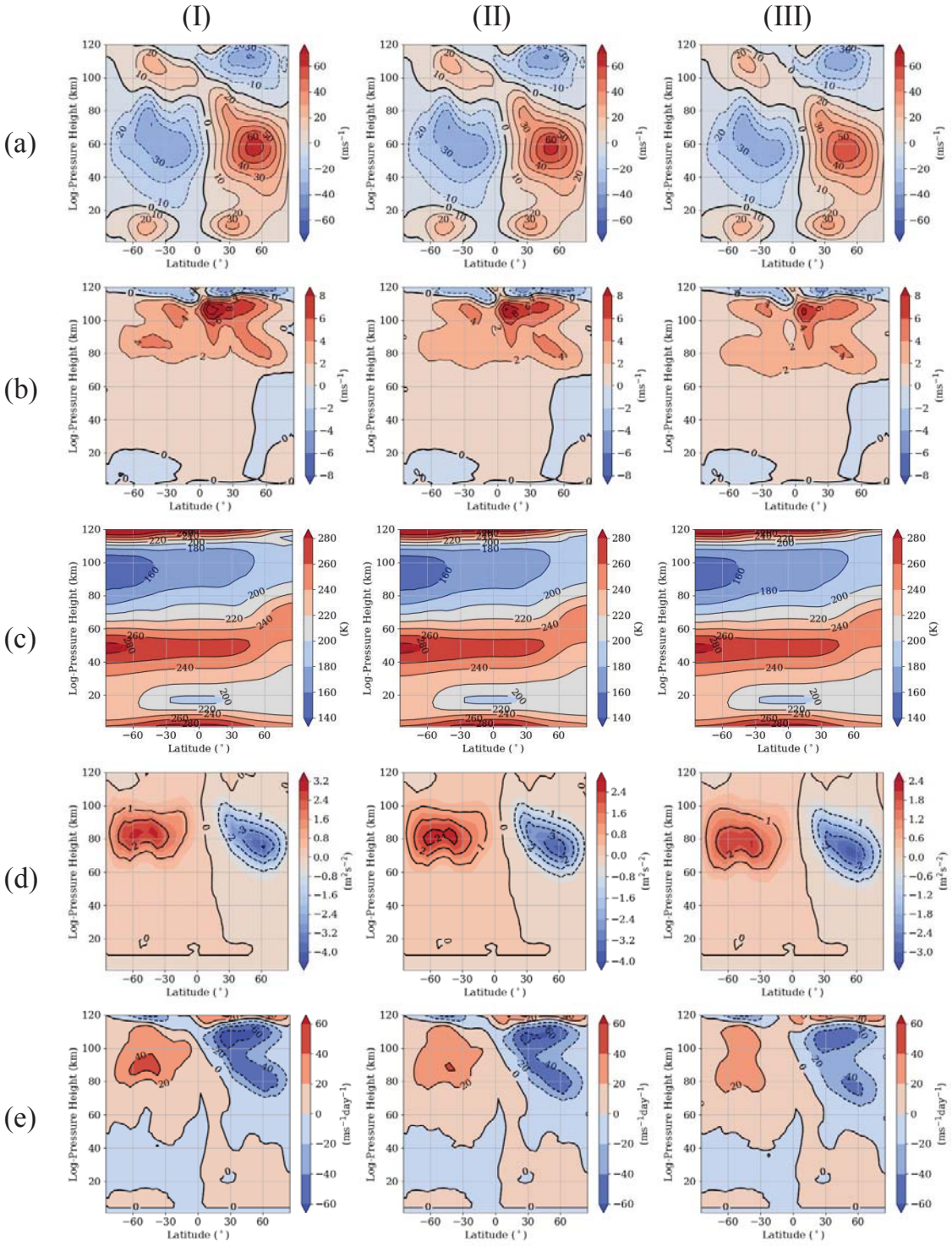

Figure 5: As in Fig. 4, but for the MF-M-C (I) MF-M-L (II) and MF-M-P (III) simulations.

Comparing I(a)-III(a) of Fig.5 shows that the zonal wind is again decreasing from 60 ms^{-1} to 50 ms^{-1} with increasing scaling factor. Also the jet maximum moves towards higher latitudes as in the EP-L-C simulation. But nevertheless, the intensity of the mesospheric jet and the height of the wind reversal are not satisfactorily reproducing observations, so that in the third approach the mean value of the variable vertical velocity perturbation was again reduced to 0.275 cms^{-1}. Results of the MF-S-C (I), MF-S-L (II) and MF-S-P (III) runs are presented in Fig. 6.

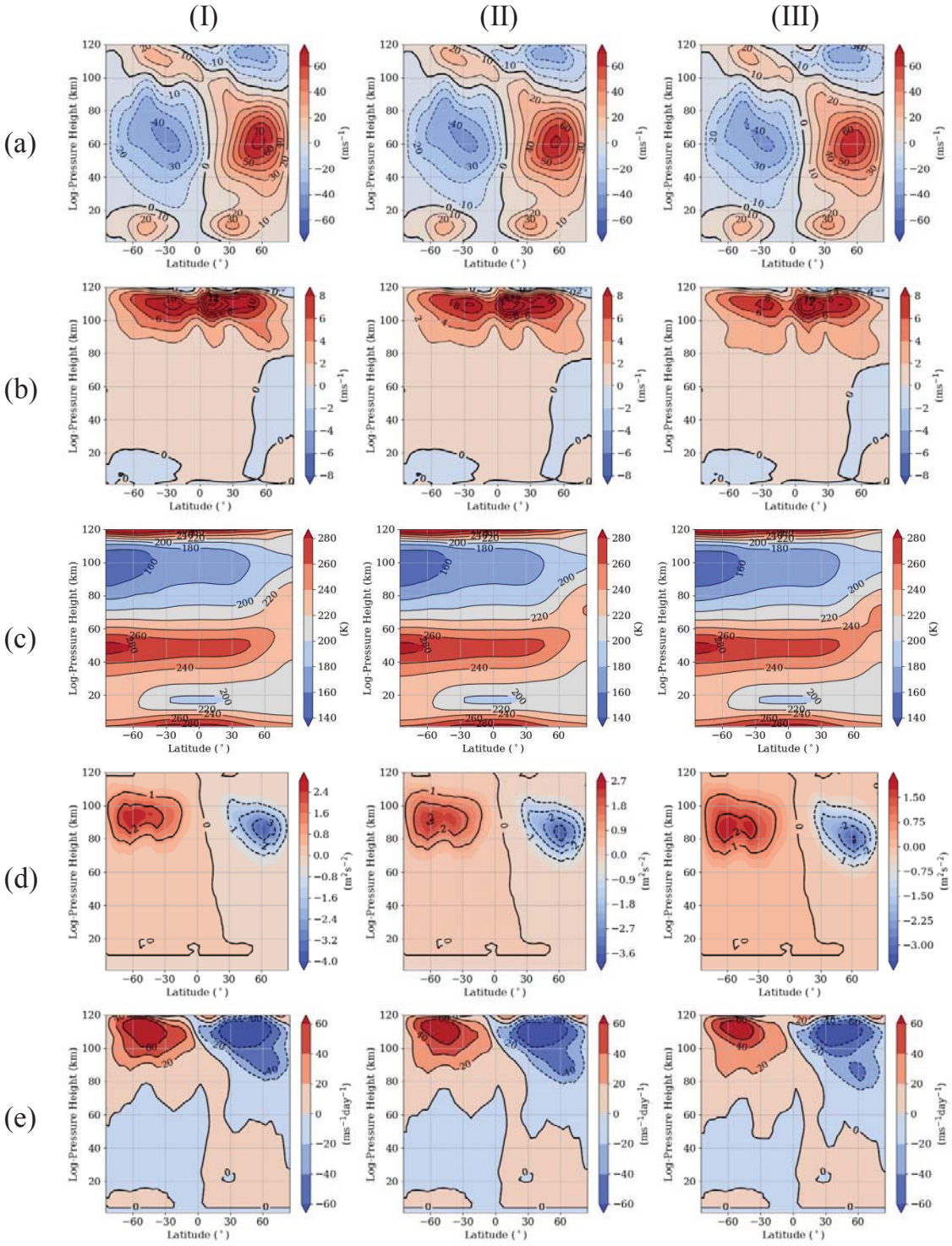

Figure 6: As in Fig. 4, but for the MF-S-C (I) MF-S-L (II) and MF-S-P (III) simulations.

Compared to the other simulations it can be directly seen that the GW flux I(d)-III(d) and the acceleration through GWs I(e)-III(e) are shifted upwards. In Fig. 6 I(a)-III(a) it can be seen that the wind reversal is now located between 90 km and 100 km which is consistent with observations (Fig. 7). But the mesospheric jet is nearly twice as strong as in the observations due to the small GWs breaking at higher altitudes. Also, the generated GWs having larger amplitudes in the linear and polynomial distribution cannot decelerate the mesospheric jet sufficiently strong. The weakest mesospheric jet can be observed in the MF-S-P simulation with a maximum of 60 ms^{-1}. In addition, the meridional circulation (Fig. 6 I(b)-III(b)) with more than 10 ms^{-1} is far too strong so that it leads to a local warming of the thermosphere (Fig. 6 I(c)-III(c)) which is not realistic. Based on these findings even the last approach does not lead to an optimal result.

5. Discussion and conclusions

In this paper we presented a new GW source distribution based on MF distributions by applying midfrequency approximation. The model experiments show that the new GW distribution is leading to a more realistic tilt of the west wind regime in the winter hemisphere towards lower latitudes with increasing height. This final outcome corresponds to the climatology illustrated in Fig. 7. This figure shows the January zonal mean zonal wind obtained from the URAP climatology [Swinbank and Ortland, 2003]. It can be seen that the mesospheric jet reaches a maximum of 40 ms^{-1} and the wind reversal is in an altitude between 90 km and 100 km. Midlatitude radar observations partly show even higher wind reversal altitudes [Jacobi, 2012]. To reproduce these characteristics a variation of large and small GWs was implemented in MUAM to decelerate the mesospheric jet by early breaking GWs with large amplitudes and to displace the wind reversal vertically by later breaking GWs with small amplitudes. A summary of all model experiments with regard to the height of the wind reversal (left) and the strength of the mesospheric jet maximum (right) is shortly summarized in Fig. 8. The height of the wind reversal was calculated for 52.5°N. It shows that the variation of the vertical velocity perturbation with a mean value of 0.275 cms^{-1} may lead to a correct altitude of the wind reversal (MF-S-P) but simultaneously, the intensity of the mesospheric jet cannot be approximately adjusted to the observations. In the reversed case, the experiment (mean of 1 cms^{-1}) may also lead to an acceptable speed of the

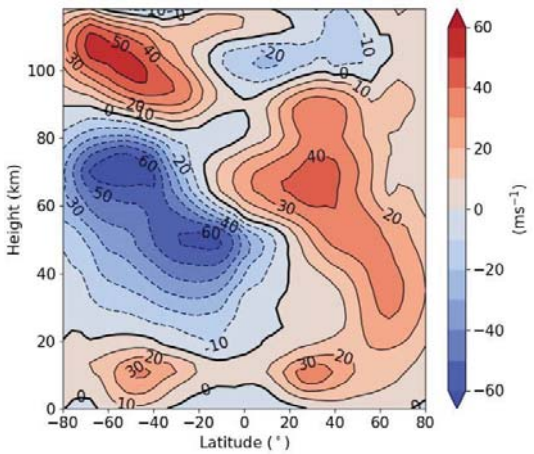

Figure 7: URAP latitude-height plot of the zonal wind [Swinbank and Ortland, 2003].

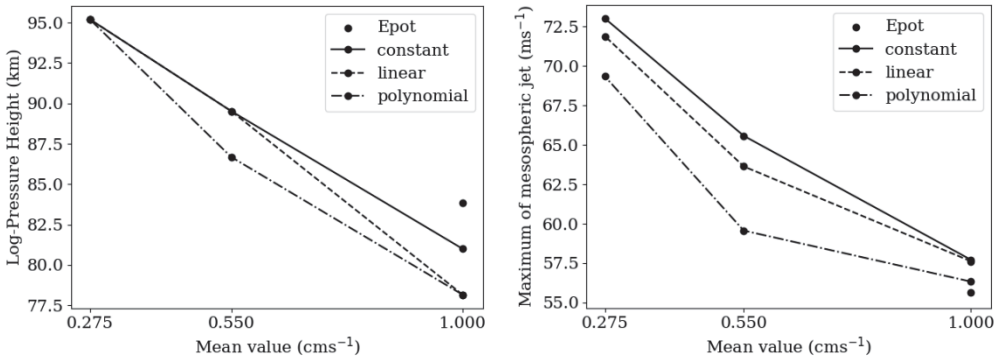

Figure 8: Overview of the height of the wind reversal at 52.5°N (left) and the strength of the mesospheric jet (right) for each simulation.

mesospheric jet (MF-L-P) but simultaneously, the wind reversal drops to lower altitudes. It may be concluded that none of the experiments provided an optimal jet with respect to both wind reversal height and intensity. It may be assumed that a composite of the simulations based on a mean of 1 cms^{-1} (MF-L-C) with a minimum of 0.05 cms^{-1} (MF-S-P) will lead to the optimal result. If this will not be the case, also the phase speed of the GWs has to be modified. Slower GWs are breaking earlier than faster GWs which means that larger GWs with smaller phase speeds are breaking at lower altitudes and may decelerate the mesospheric jet.

Acknowledgements

This study has been supported by Deutsche Forschungsgemeinschaft (DFG) under the grant JA836/32-1. ECMWF reanalysis data are provided by apps.ecmwf.int/datasets/data/. We acknowledge support by P. Šácha, Charles University Prague, for providing GW potential energy distributions.

References

Baumgarten, G., Fiedler, J., Hildebrand, J. and Lübken, F.-J., 2015: Inertia gravity wave in the stratosphere and mesosphere observed by Doppler wind and temperature lidar, Geophys. Res. Lett., 42, 10,929-10,936, https://doi.org/10.1002/2015GL066991.

Ern, M., Preusse, P., Alexander, M. J. and Warner, C. D., 2004: Absolute values of gravity wave momentum flux derived from satellite data, J. Geophys. Res., 109, D20103, https://doi.org/10.1029/2004JD004752.

Fleming, E. L., Chandra, S., Barnett, J. J. and Corney, M., 1990: Zonal mean temperature, pressure, zonal wind and geopotential height as functions of latitude, Adv. Space Res., 10, 12. (12)11-(12)59, https://doi.org/10.1016/0273-1177(90)90386-E.

Fomichev, V. I., Blanchet, J.-P. and Turner, D. S., 1998: Matrix parameterization of the 15 mm CO2 band cooling in the middle and upper atmosphere for variable CO2 concentration, J. Geophys. Res., 103, 11.505–11.528, https://doi.org/10.1029/98JD00799.

Fritts, D. C. and Alexander, M. J., 2003: Gravity wave dynamics and effects in the middle atmosphere, Rev. Geophys., 41, 1003, https://doi.org/10.1029/2001RG000106, 1.

Fröhlich, K., Pogoreltsev, A., Jacobi, Ch., 2003a: The 48-layer COMMA-LIM model, Rep. Inst. Meteorol. Univ. Leipzig, 30, 157-185, http://nbn-resolving.de/urn:nbn:de:bsz:15-qucosa-217766.

Fröhlich, K., Schmidt, T., Ern, M., Preusse, P., de la Torre, A., Wickert, J. and Jacobi, Ch., 2007: The global distribution of gravity wave energy in the lower stratosphere derived from GPS data and gravity wave modelling: attempt and challenges, J. Atmos. Sol.-Terr. Phys., 69, 2238-2248, https://doi.org/10.1016/j.jastp.2007.07.005.

Gavrilov N. and Fukao, S., 1999: The MU radar measurements and modeling of the gravity wave climatology and sources in the atmosphere, Adv. Space Res., 24 ,565-574, https://doi.org/10.1016/S0273-1177(99)00202-1.

Hertzog, A., Alexander, M. J. and Plougonven, R., 2012: On the Intermittency of Gravity Wave Momentum Flux in the Stratosphere. J. Atmos. Sci., 69, 3433–3448, , https://doi.org/10.1175/JAS-D-12-09.1.

Holton, J. R., 1982: The role of gravity wave induced drag and diffusion in the momentum budget of the mesosphere, J. Atmos. Sci., 39, 791-799, https://doi.org/10.1175/1520-0469(1982)039<0791:TROGWI>2.0.CO;2.

Jacobi, Ch., F. Lilienthal, C. Geißler, and A. Krug, 2015: Long-term variability of mid-latitude mesosphere-lower thermosphere winds over Collm (51°N, 13°E), J. Atmos. Sol.-Terr. Phys., 136, B, 174-186, https://doi.org/10.1016/j.jastp.2015.05.006.

Jacobi, Ch., 2012: 6 year mean prevailing winds and tides measured by VHF meteor radar over Collm (51.3°N, 13.0°E), J. Atmos. Sol.-Terr. Phys., 78-79, 8-18, https://doi.org/10.1016/j.jastp.2011.04.010.

Jacobi, Ch., Fröhlich, K. and Pogoreltsev, A., 2006: Quasi two-day-wave modulation of gravity wave flux and consequences for the planetary wave propagation in a simple circulation model, J. Atmos. Sol.-Terr. Phys., 68, 283-292, https://doi.org/10.1016/j.jastp.2005.01.017.

Jakobs, H. J., Bischof, M., Ebel, A., Speth, P., 1986: Simulation of gravity wave effects under solstice conditions using a 3-D circulation model of the middle atmosphere, J. Atmos. Terr. Phys., 48, 1203-1223, , https://doi.org/10.1016/0021-9169(86)90040-1.

Lilienthal, F., Jacobi, Ch., Schmidt, T., de la Torre, A. and Alexander, P., 2017: On the influence of zonal gravity wave distributions on the Southern Hemisphere winter circulation, Ann. Geophys., 35, 785-798, https://doi.org/0.5194/angeo-35-785-2017.

Lindzen, R. S., 1981: Turbulence and stress owing to gravity wave and tidal breakdown, J. Geophys. Res., 86, 9707-9714, https://doi.org/10.1029/JC086iC10p09707.

Oleynikov, A.N., Jacobi, Ch. and Sosnovchick, D.M., 2005: Parameters of internal gravity waves in the mesosphere-lower thermosphere region derived from meteor

radar wind measurements, Ann. Geophys., 23, 3431-3437, https://doi.org/10.5194/angeo-23-3431-2005.

Plougonven, R., Hertzog, A. and Guez, L., 2013: Gravity waves over Antarctica and the Southern Ocean: consistent momentum fluxes in mesoscale simulations and stratospheric balloon observations, Q.J.R. Meteorol. Soc., 139, 101–118, https://doi.org/10.1002/qj.1965.

Pogoreltsev, A. I., Vlasov, A. A., Fröhlich, K., und Jacobi, C., 2007: Planetary waves in coupling the lower and upper atmosphere, J. Atmos. Solar-Terr. Phys., 69, 2083-2101, https://doi.org/10.1016/j.jastp.2007.05.014.

Preusse, P., Ern, M., Eckermann, S. D., Warner, C. D., Picard, R. H., Knieling, P., Krebsbach, M., Russell, J. M., Mlynczak, M. G., Mertens, C. J. and Riese, M., 2006: Tropopause to mesopause gravity waves in August: Measurement and modeling, J. Atmos. Sol.-Terr. Phys., 68, 1730-1751, https://doi.org/10.1016/j.jastp.2005.10.019.

Ratnam, M.V., T. Tsuda, Ch. Jacobi, and Y. Aoyama, 2004a: Enhancement of gravity wave activity observed during a major Southern Hemisphere stratospheric warming by CHAMP/GPS measurements, Geophys. Res. Lett., 31, L16101, https://doi.org/10.1029/2004GL019789.

Ratnam, M.V., Tetzlaff G. and Jacobi, Ch., 2004b: Global and seasonal variations of stratospheric gravity wave activity deduced from the CHAllenging Minisatellite Payload (CHAMP)-GPS Satellite, J. Atmos. Sci., 61, 1610-1620, https://doi.org/10.1175/1520-0469(2004)061<1610:GASVOS>2.0.CO;2.

Šácha, P., Kuchar, A., Jacobi, Ch. and Pišoft, P., 2015: Enhanced internal gravity wave activity and breaking over the Northeastern Pacific / Eastern Asian region, Atmos. Chem. Phys., 15, 13097-13112, https://doi.org/10.5194/acp-15-13097-2015.

Šácha, P., F. Lilienthal, Ch. Jacobi, and P. Pišoft, 2016: Influence of the spatial distribution of gravity wave activity on the middle atmospheric circulation and transport, Atmos. Chem. Phys., 16, 15755-15775, https://doi.org/10.5194/acp-16-15755-2016.

Schmidt, T., P. Alexander, and A. de la Torre, 2016: Stratospheric gravity wave momentum flux from radio occultations, J. Geophys. Res. Atmos., 121, 4443–4467, https://doi.org/10.1002/2015JD024135.

Strobel, D. F., 1986: Parameterization of the atmospheric heating rate from 15 to 120km due to O2 and O3 Absorption of solar radiation, J. Geophys. Res., 83:6225–6230. https://doi.org/10.1029/JC083iC12p06225.

Witschas, B., Rahm, S., Dörnbrack, A., Wagner, J. and Rapp, M., 2017: Airborne Wind Lidar Measurements of Vertical and Horizontal Winds for the Investigation of Orographically Induced Gravity Waves, J. Atmos. Oceanic Technol., 34, 1371–1386, https://doi.org/10.1175/JTECH-D-17-0021.1.